Mine Water Environ (2017) 36:550–563
DOI 10.1007/s10230-017-0444-6

TECHNICAL ARTICLE

Delineating the Origin of Groundwater in the Golgohar Mine Area of Iran Using Stable Isotopes of ^{2}H and ^{18}O and Hydrochemistry

Reza Jahanshahi[1,2] · Mohammad Zare[1]

Received: 5 April 2016 / Accepted: 16 February 2017 / Published online: 29 March 2017

Abstract The Golgohar iron ore mine in southern Iran is a large open pit that uses dewatering (≈4000–5000 m^3/day) to prevent flooding. A vast cone of depression has formed, and water from a large area flows into the pit. A study of the different sources of this water was necessary to plan a proper dewatering project. Moreover, the discharged water is saline and contains high levels of contaminants. Based on hydrochemical and isotope (^{18}O and ^{2}H) analysis, it was concluded that the area's deep saline groundwater is coming from the Sirjan (Kheirabad) salt playa (north of the mine) by saltwater intrusion while the chemistry of more distant groundwater was due to dissolved minerals.

Keywords Salinity · Dewatering · Mine pit · Sirjan salt playa

Introduction

Factors such as geology, mineralogy, and geochemical processes within an aquifer typically control groundwater composition. Water quality changes due to processes such as: evaporation, mixing of waters, cation exchange, mineral dissociation, oxidation/reduction, and secondary mineral precipitation (Appelo and Postma 2005). Chemical and isotopic indicators have been used to trace flow systems, determine origins of groundwater salinity, observe migration of the fresh–salt water interface, and understand mixing of saline and fresh water (Allen and Lepitre 2004; Cartwright et al. 2006; Dixon and Chiwell 1992; Faye et al. 2005; Gammons 2006; Gammons et al. 2006; Ghiglieri et al. 2012; Giménez and Morell 1997; Han et al. 2011; Jahanshahi and Zare 2016; Magaritz and Luzier 1985; Mohammadi et al. 2012; Möller et al. 2007; Mondal et al. 2011; Singh et al. 2011; Morell et al. 1996; Tijani 2004; Yidana and Yidana 2010; Zhang et al. 2007). Salinity can be used to determine the origin of groundwater because evaporated sea water, connate waters, and waters affected by evaporite dissolution are high in total dissolved solids (TDS), chloride, and salinity, and relatively low in bicarbonates (Amajor and Gbadebo 1992). However, one cannot differentiate water with the same salinity and different origins in this way, so ion ratios Na/Cl, Cl/Br, Ca/SO_4, Ca/HCO_3, $Ca+Mg/\ SO_4+HCO_3$ have been used to distinguish possible groundwater origins (Faye et al. 2005; Ghiglieri et al. 2012; Mohammadi et al. 2012; Möller et al. 2007; Mondal et al. 2011; Tijani 2004; Yidana and Yidana 2010).

Sources of dissolved Cl^- in groundwater include salt water intrusion, mineral dissolution (principally halite), chloride buried during sediment deposition, marine aerosols, oil and gas-field brines, agriculture, and industrial effluents (Park et al. 2005). The Na/Cl ratio can be used to distinguish brine produced by halite dissolution from oil field brine. Generally, oil field brines have Na/Cl molar ratios much less than 1 (Richter and Kreitler 1993).

The Cl/Br ratio is also useful (Alcalá and Custodio 2008; Cartwright et al. 2006; Freeman 2007; Iribar andÁ balos 2011; Leybourne and Goodfellow 2007). When seawater

Electronic supplementary material The online version of this article (doi:10.1007/s10230-017-0444-6) contains supplementary material, which is available to authorized users.

✉ Mohammad Zare
zare@susc.ac.ir

Reza Jahanshahi
jahanshahireza@science.usb.ac.ir

[1] Department of Earth Sciences, Shiraz University, Shiraz, Iran

[2] Department of Geology, University of Sistan and Baluchestan, Daneshgah St., Zahedan, Iran

initially evaporates, Cl^- and Br^- concentrations increase in the residual hypersaline waters, but the Cl/Br ratio does not change; however, when halite begins to precipitate, a small fraction of the bromide is absorbed in the halite lattice, while the Cl^- precipitates as a halite component. Since Br^- is more soluble than Cl^-, this ratio of the residual water decreases with progressive evaporation; therefore, halite dissolution produces waters with a high Cl/Br ratio (Carpenter 1978; Kharaka et al. 1987).

The stable isotopes of ^{18}O and ^{2}H are also often used to identify groundwater sources (Currell Matthew et al. 2014; Faye et al. 2005). When no significant evaporation of rainwater occurs before and after infiltration, concentrations of these isotopes remain unchanged, and the groundwater follows the precipitation pattern of the area. Moreover, they can be used to differentiate between evaporation and mineral dissolution. Variations in the stable isotopic composition of groundwater can be caused by: (1) natural variations in the isotopic composition of precipitation, (2) mixing of different waters, and (3) evaporation (Faye et al. 2005; Sprenger et al. 2014). Bahim et al. (2015) used δ^2H and $\delta^{18}O$ and chemical analyses to differentiate alluvial and deep aquifers and demonstrate a local recharge source for the alluvial aquifer.

The Golgohar iron ore mine in southern Iran is a large open pit that uses dewatering (≈4000–5000 m^3/day) to prevent flooding. A vast, deep cone of depression has formed, and water from all around the area and a deep aquifer flows into the pit. New wells continue to be drilled inside and outside of the pit to prevent flooding and/or reduce its magnitude. However, understanding the origin of the groundwater and differentiating different water sources is necessary to improve dewatering. In addition, the salinity of the discharged water from the pit and the area's groundwater is high. Hydrochemistry and

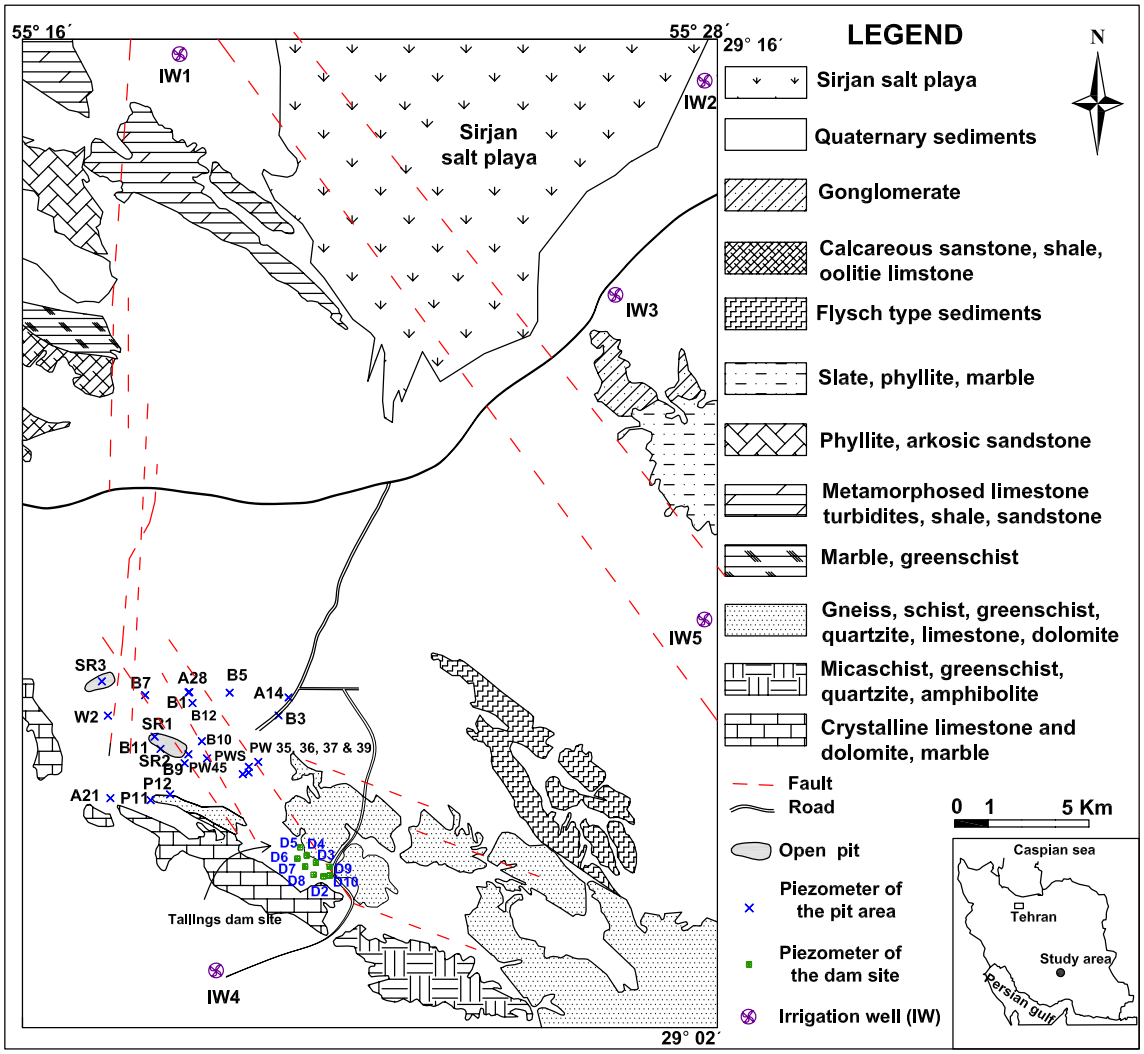

Fig. 1 Geological map of the study area and sampling points

Table 1 Field measurements, analytical data and saturation indices of calcite, dolomite, gypsum and halite (concentrations and TDS are expressed in mg/L and EC in μmhos/cm)

Sample location	Sample	EC	pH	HCO_3^-	Cl^-	SO_4^{2-}	Ca^{2+}	Mg^{2+}	Na^+	K^+	Br^-	TDS	SI_{cal}	SI_{dol}	SI_{gyp}	SI_{hal}
Pit area sample	A14	32,500	7.42	48	18,282	2417	6650	210	4554	45	22.58	32,207	0.65	0.2	0.42	−1.35
	A15	7840	7.27	115	3319	990	610	234	1175	6	–	6452	0.24	0.43	−0.41	−2.57
	A21	7750	7.02	24	3017	611	460	198	1265	8	2.17	5584	0.11	−1.62	−0.68	−2.57
	A28	27,000	7.3	73	11,892	1732	3050	420	4002	17	11.64	21,187	0.5	0.53	0.1	−1.57
	B1	77,700	6.3	24.4	48,812	785	10,750	150	17,296	72	35.16	77,891	1.3	1.8	0.6	−0.71
	B3	17,300	7.74	79	6833	3545	1510	204	3864	22	3.42	16,058	0.65	0.8	0.24	−1.81
	B5	59,200	7.81	73	32,926	2739	10,450	540	8002	65	38.56	54,797	1.27	1.69	0.52	−0.86
	B7	21,100	7.43	91	9585	1873	2250	390	3519	20	9.06	17,728	0.6	0.83	0.08	−1.71
	B9	9290	7.36	85	3230	2437	770	186	1955	10	1.94	8674	0.21	0.16	−0.02	−2.38
	B10	50,800	7.32	54	29,997	1228	7100	300	10,166	42	28.74	48,889	0.6	0.26	0.09	−0.8
	B11	12,940	7.45	67	5058	2981	1176	326	2622	10	3.77	12,241	0.33	0.45	0.12	−2.09
	B12	8200	7.54	91	2485	2175	570	180	1610	7	1.94	7118	0.24	0.33	−0.14	−2.56
	P11	12,830	7.33	103	4526	1748	710	228	2346	10	2.31	9672	0.18	0.23	−0.21	−2.16
	P12	20,400	7.76	103	9318	1795	2040	324	4119	33	7.77	17,735	1	1.58	0.03	−1.65
	PW35	18,140	6.85	61	8875	1537	2180	336	3105	16	6.41	16,111	0.06	−0.54	0.01	−1.79
	PW36	17,260	7.42	79	7543	1814	1800	342	2875	16	6.54	14,471	0.48	0.62	0.03	−1.89
	PW37	15,610	8.11	48	7455	1146	2080	246	2415	18	7.19	13,409	0.98	1.42	−0.09	−1.96
	PW39	16,340	6.82	36	7277	2426	2100	228	2898	21	7.14	14,988	−0.4	−1.38	0.21	−1.9
	PWS	44,600	7.06	48	25,116	2397	6250	270	8970	37	21.08	43,089	0.32	−0.31	0.36	−0.93
	W2	8950	7.77	91	3053	2598	500	306	2001	18	1.67	8568	0.44	1.01	−0.18	−2.4
Seepage water in pit 1 and pit 3	S1	9570	7.88	73	3461	2457	720	228	2093	9	2.45	9041	0.59	1.03	−0.06	−2.33
	S2	32,200	7.61	48	16,418	2618	3600	870	5681	35	14.71	29,272	0.61	1.01	0.24	−1.3
	S3	38,500	7.44	61	20,412	1631	4150	630	7751	18	15.99	34,654	0.58	0.75	0.08	−1.07
Irrigation well sample	IW1	8950	7.23	152	2662	219	270	132	1027	10	0.58	4475	0.03	0.11	−1.22	−2.69
	IW2	8860	7.25	149	2660	221	271	128	1012	9	–	11,540	0.03	0.12	−1.20	−2.71
	IW3	13,940	7.30	134	6212	1856	890	414	2034	13	0.67	11,555	0.36	0.75	−0.16	−2.1
	IW4	5230	7.36	109	2023	374	300	216	613	5	1.31	3642	0.13	0.47	−0.97	−3.02
	IW5	1887	7.64	262	330	705	88	9	335	9	–	1826	0.92	1.53	−0.47	−4.04
Dam site area sample	D2	3480	7.61	189	710	955	140	66	667	8	0.95	2735	0.22	0.47	−0.78	−3.42
	D3	4310	7.65	250	692	1662	96	62	1035	10	1.38	3808	0.18	0.51	−0.81	−3.27
	D4	4580	7.49	239	781	1585	156	50	943	9	1.59	3764	0.18	0.21	−0.62	−3.25
	D5	3840	7.5	231	656	1512	180	72	510	7	1.57	3170	0.25	0.44	−0.54	−3.58
	D6	6440	7.4	176	1782	1877	332	192	1252	10	1.55	5623	0.23	0.58	−0.36	−2.8
	D7	5560	7.34	195	1420	1547	264	105	1173	10	1.25	4716	0.12	0.18	−0.47	−2.91
	D8	4670	7.34	225	1029	1662	200	84	1081	10	1.53	4292	0.06	0.08	−0.53	−3.08
	D9	4260	7.49	305	408	1967	88	79	1035	11	1.82	3894	0.01	0.3	−0.81	−3.5
	D10	1306	7.86	701	216	263	50	30	201	12	0.05	1476	0.81	1.74	−1.53	−4.4
Sirjan salt playa	SM	457,000	6.67	30	200,575	1525	6100	3360	121,882	424	–	333,900	0.41	1.25	−0.01	−0.10

stable isotope composition were used to investigate the effects of dewatering and the origins of the salinity.

Description of the Study Area

The Golgohar iron ore mine is located about 50 km southwest of the town of Sirjan, in Kerman province (55°15′–55°24′N and 29°03′–29°07′E), in an area of planar desert topography. The area is generally covered by Neogene conglomerates and Quaternary deposits; exposed rocks include biotite schist, amphibolite, granite, and marbles. Metamorphism obliterated the original textures and converted the sediments into magnetite, skarn, amphibolite, gneiss, schist, and Ca–Mg carbonate marble. Other minerals include calcite, dolomite, quartz, feldspars, biotite, muscovite–sericite, talc, epidote, zoisite, chlorite, tremolite–actinolite, hornblende, and spinel. Quaternary sediments of alluvial fans, talus, and river sediments dominate the area (Mücke and Younessi 1994).

The area is semiarid with an average annual rainfall of 172 mm (mainly in the winter); potential evaporation exceeds precipitation for much of the year. The highest temperature recorded was +40 °C, the lowest temperature was 16 °C, and the relative humidity averages about 33%.

The Golgohar area is surrounded by the Sirjan salt playa in the north and the Marg (death) salt salt playa in the south. Sediments of the salt plains are a mixture of clay, salt, and gypsum and the land in both plains becomes swampy during the rainy season.

The mine contains six ore bodies spread over an area of 40 square km. Only ore deposit (pit 1) is currently being extracted; dewatering is also going on. Overburden extraction is proceeding at deposit number 3 (pit 3), with only limited pumping of seepage. A tailings dam is under construction south of the mine for the mine wastes.

Hydrogeological study of the mine area indicates that two aquifers exist; the upper aquifer is an alluvial aquifer located above a hard (metamorphic) rock aquifer. Since there is no impermeable layer between the aquifers, the two are hydraulically connected. Quality of groundwater in the area is very low (the average electrical conductivity (EC) nearly is 15,000 μmhos/cm) and is not suitable for drinking water. In parts of the region, groundwater is used to irrigate pistachio farms (a saline resistant crop).

Materials and Methods

Sample Collection and Analysis

Altogether, the 38 duplicate water samples that were collected (at July 2011) for hydrochemical analysis were sorted into four sets: set I, groundwater from piezometers and pumping wells around pits 1 and 3 and pit floor seepage, which are referred to here as the "pit area samples"; set II, groundwater from piezometers at the site of the proposed tailings dam, which are referred to as the "dam site samples"; set III, samples from irrigation wells around the Sirjan salt playa (three wells) north and northeast of the mine, an irrigation well south of the mining area near Marg salt playa (one well), and a drinking water well east of the mine area, which are all referred to as irrigation well samples; and set IV, a water sample from the Sirjan salt marsh. Figure 1 shows the location of the sampling points. Samples were stored in acid-washed, polyethylene bottles that were thoroughly rinsed with representative water samples, transferred to the laboratory in a short time, and stored in a refrigerator. Temperature, EC, and pH were measured in situ using pre-calibrated portable digital EC (WTW LF191) and pH (Jenway) meters. In the laboratory, samples were filtered to remove suspended sediment, then divided in two aliquots: one was used for analysis of major anions, while the second were treated with 1 mL of concentrated HNO_3 used for major cation analysis. Major ions were analyzed employing standard methodologies (APHA 1989): Cl^- by standard $AgNO_3$ titration; HCO_3^- by titration with HCl, SO_4^{2-} was determined by spectrophotometric turbidimetry (HACH model of Ratio/XR, 43900); Mg^{2+} and Ca^{2+} by titration using standard EDTA; Na^+ and potassium K^+ by flame photometry (Perkin-Elmer model of Coleman, S1-A); Br^- content via ion chromatography; and TDS was determined gravimetrically at 105–110 °C in the hydrochemistry laboratory of the

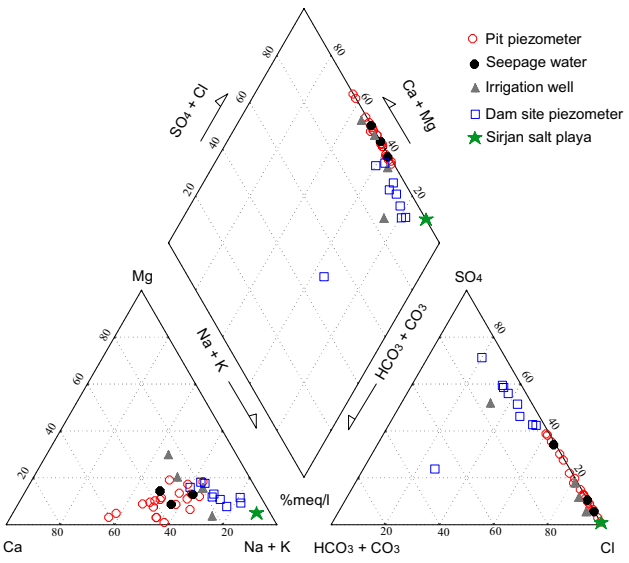

Fig. 2 Piper plot for water samples of the study area to determine the dominant water facies

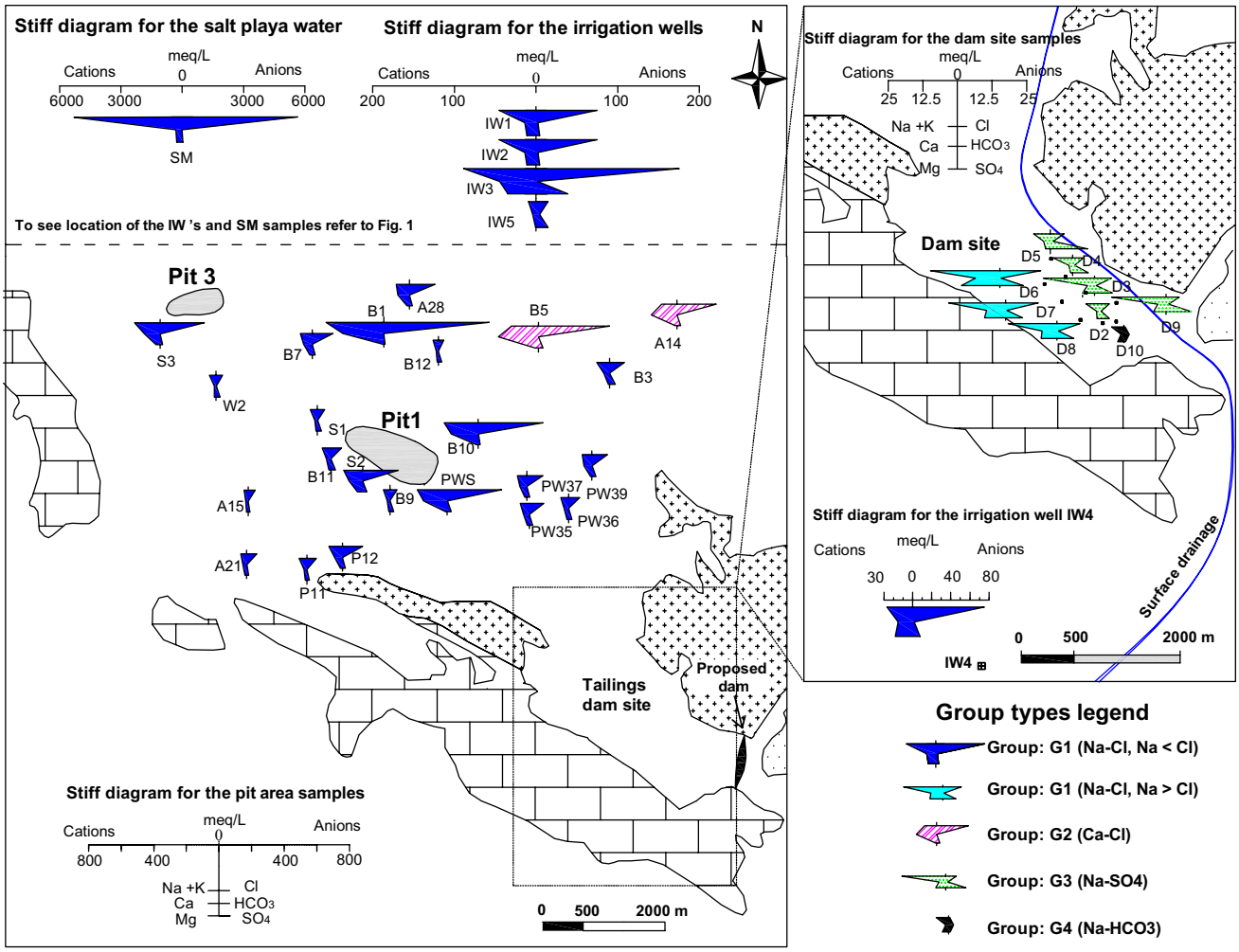

Fig. 3 Stiff diagram of water samples; ploted position of the Sirjan salt playa (SM) and irrigation wells (IW's) are not to scale

Dept. of Earth Sciences, Shiraz University. The quality of the analyses was evaluated using the electrical balance equation; samples with more than a 5% difference were re-analyzed (Appelo and Postma 2005).

Groundwater samples from the locations mentioned above and precipitation samples from three different topographic elevations were collected in dark bottles and stored in a refrigerator before being sent to the Freie University laboratory in Berlin, Germany for analysis of $\delta^2H‰$ and $\delta^{18}O‰$, relative to the VSMOW standard.

Results and Discussion

Hydrochemistry

The physicochemical properties of the samples are given in Table 1. The pH of the water samples ranged from 6.3 to 8.11. The EC ranged from 1306 to 457,000 μmhos/cm (TDS ranged between 1476 and 333,900 mg/L). The relative weight of Cl^-, the dominant anion in most water samples, ranged from 10 to 62% of the total weight of anions. The predominant anion at the proposed tailings dam site was sulphate. The dominant cation of most of the samples was Na^+, with relative weight ranges from 8 to 36%.

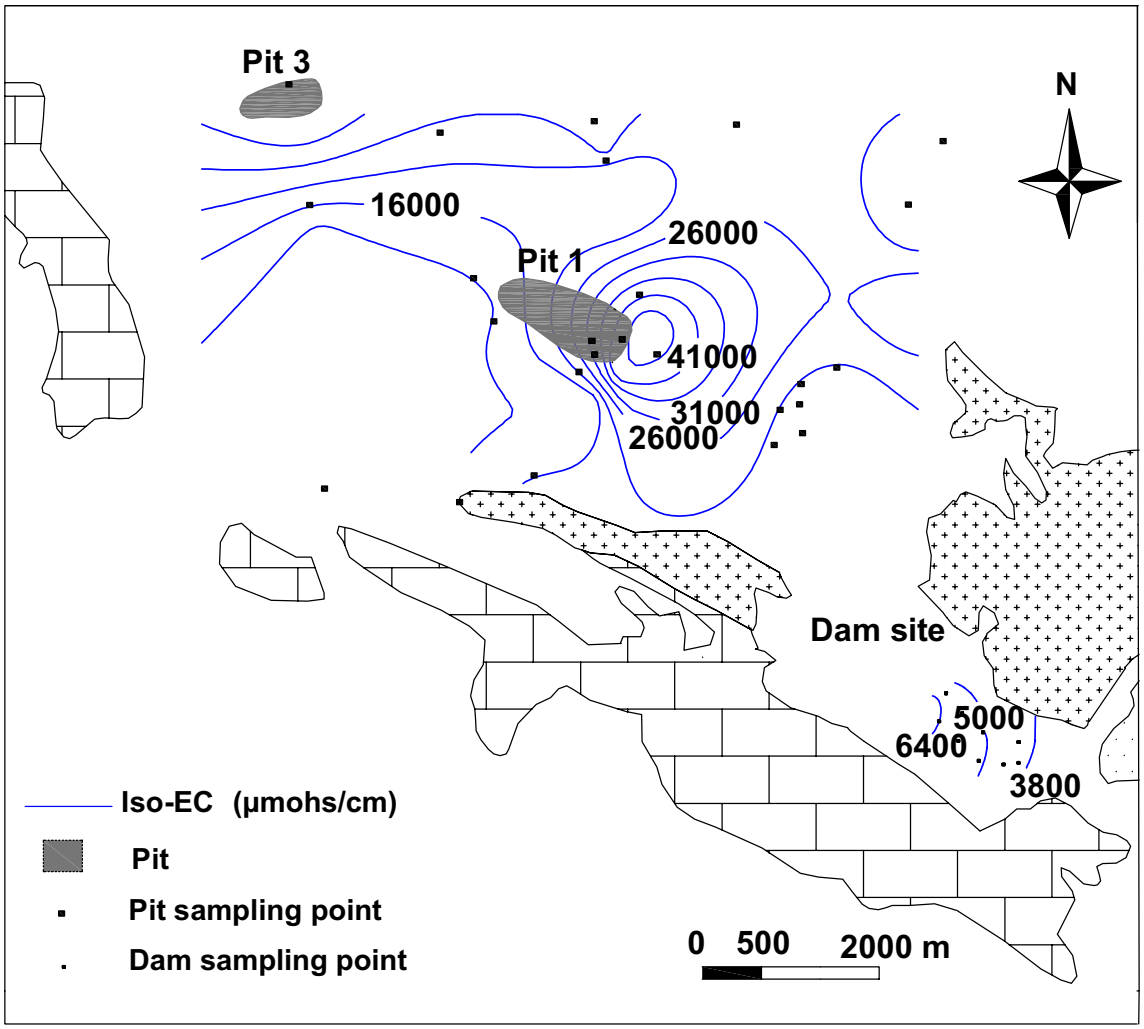

Fig. 4 Iso-EC map in the pit and dam site area

Water Types

All of the samples were plotted as Piper (Fig. 2) and Stiff (Fig. 3) diagrams to determine the dominant water facies in the aquifer. Samples were then categorized into four "water types"; i.e. Na–Cl (group G1), Ca–Cl (group G2), Na–SO_4 (group G3), and Na–HCO_3 (group G4). The pit area samples were mostly G1, with the exception of two samples (B5 and A14) from the northeastern part of the pit, which were G2. The weak domination of Ca^{2+} over Na^+ in B5 and A14 could be due to cation exchange. Samples from the dam site (samples D6, D7, and D8) grouped in G1, with $Na^+ > Cl^-$; samples D2, D4, D5, and D9, located close to exposed metamorphic rocks, near a drainage channel that transports surface runoff from the area, were G3; and sample D10 was G4. The irrigation wells (IW1-IW5), which were far from the pits and the Sirjan salt playa water (Fig. 1), were type G1 (Fig. 3).

Iso-concentration Map of the Ions

To investigate the spatial distribution and factors affecting the chemical composition of the waters, iso-concentration maps of EC, Cl^-, Na^+, Ca^{2+} and SO_4^{2-} (Figs. 4, 5) were compared with the iso-potential and groundwater flow. The flow pattern and groundwater potential head of the pit area differ from the dam site (Fig. 6). Due to dewatering, a vast cone of depression has developed, causing groundwater to move from the Sirjan salt playa towards the pit. Flow of groundwater at the dam site is from north to south and it seems that the dewatering has not affected the dam site groundwater yet. On the other hand, Figs. 4 and 5a, b indicate that EC, Cl^-, and Na^+ in the groundwater of the pit

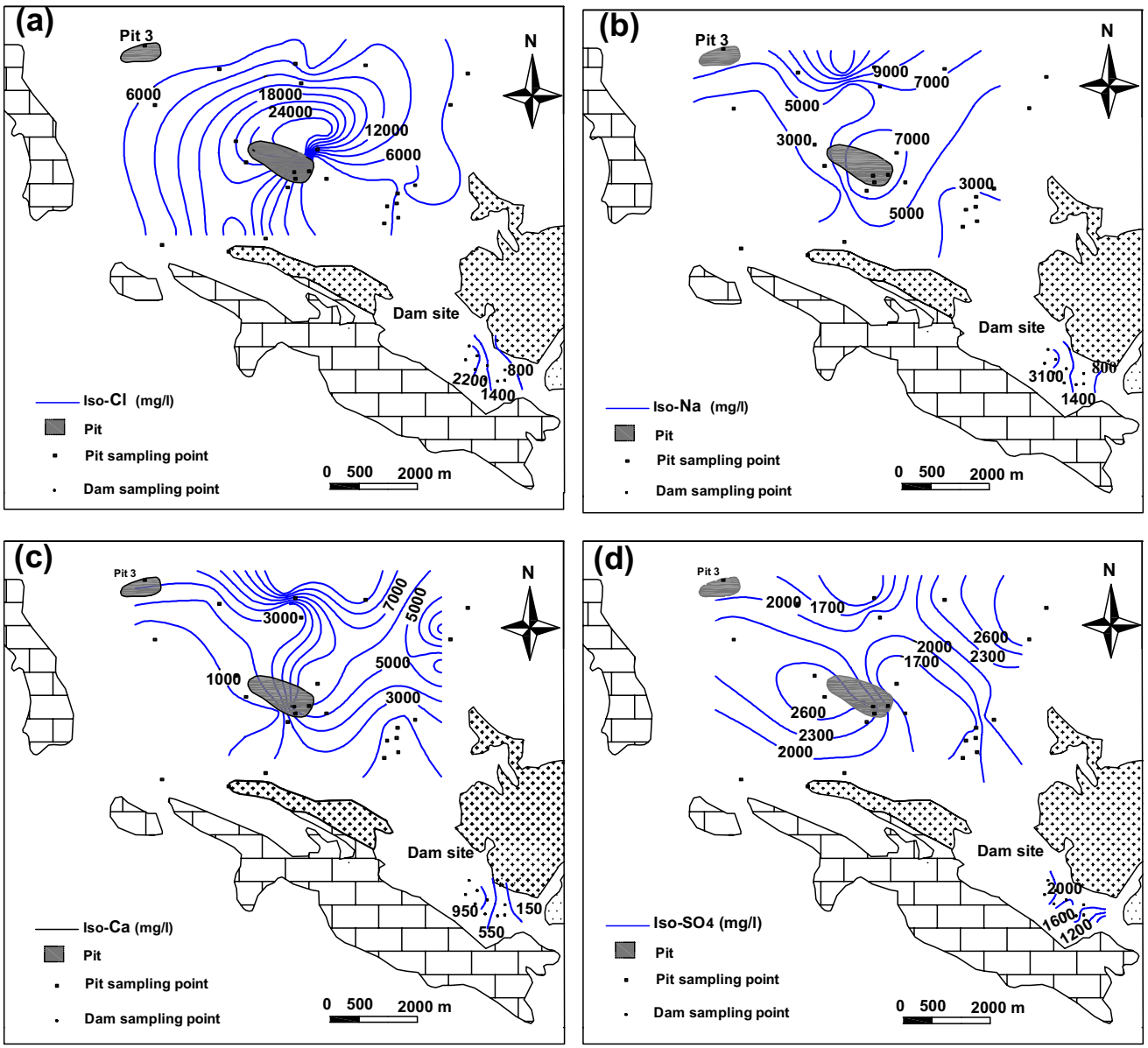

Fig. 5 Iso-ion concentration map in the pit and dam site area: **a** Cl^-, **b** Na^+, **c** Ca^{2+}, **d** SO_4^{2-}

area generally increase toward the pit; their iso-concentration patterns are relatively similar to the groundwater flow pattern. Since, $Cl^-$and Na^+ are the dominant ions, their concentration contour lines almost mirror the EC contours. These iso-values were generally less at the dam site than in the pit area.

The Ca^{2+} and SO_4^{2-} concentrations in the mine area groundwater (Figs. 5c, 7d) differ from the groundwater potential head pattern. This implies that other factors, like dissolution of calcite, dolomite, and gypsum, pyrite oxidation, and ion exchange have affected Ca^{2+} and SO_4^{2-} concentrations. Figure 5c also shows that concentrations of Ca^{2+} in the groundwater of the dam site increase from the east to the west of the site; this is probably due to the presence of calcite and dolomite in west and south of the site. The SO_4^{2-} map (Fig. 5d) shows a different pattern, increasing from the southeast towards the northwest, for no known reason.

Ion Ratios

To deliberate deeper into the different concentration patterns and investigate the sources of the various ions, molar ratios were calculated (supplemental Table 1). The ratio of Na/Cl versus Cl^- (Fig. 7a) indicates that this ratio was less than one for all samples from the pit area and the irrigation

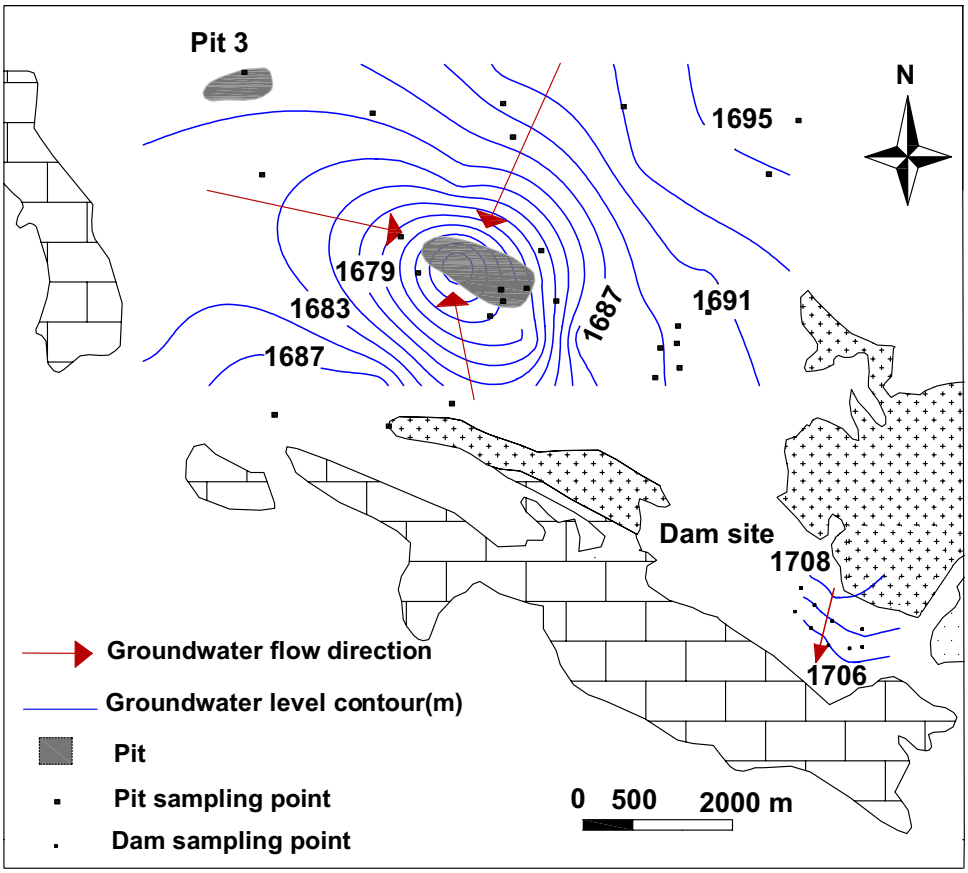

Fig. 6 Groundwater iso-potential map and flow direction in the pit and dam site area

wells (except for IW5, which had a relatively low EC and is used as drinking water) and is above one for samples from the dam site. One would expect a ratio of one if these ions were solely due to halite dissolution. Dissolution of other minerals and cation exchange would have changed this ratio. Since Cl^- is a relatively conservative ion, the decreased ratio could be due to 'reverse' cation exchange, favoring the right side of the equation shown below (Appelo and Postma 2005):

$$Na^+ + \tfrac{1}{2}\,Ca - X_2 \leftrightarrow Na - X + \tfrac{1}{2}\,Ca^{2+}$$

Dissolution of sodium-bearing minerals and/or 'direct' cation exchange (the left-hand side of the above equation), will increase the ratio. Considering samples from the pit and irrigation wells (IW1-4) close to the Sirjan salt marsh, with Na/Cl < 1, we can deduce that water from the salt playa (SM sample, with a Na/Cl ration of 0.94) moves towards the pit and irrigation wells and that the ratio changes due to reverse cation exchange. However, for samples from the dam site and IW5, the excess Na^+ could be due to weathering and dissolution of sodium silicate (Möller et al. 2007) or direct cation exchange.

The less saline dam site samples had higher ratios of K/Cl and Mg/Cl (supplemental Table 1, Fig. 7b, c) versus Cl^- than the more saline pit area waters. This could be due to weathering of the more resistant silicate minerals in the dam area, while groundwater from the pit area is influenced by the sedimentary material in the pit area and groundwater from the salt marshes. The molar ratio of Ca/Cl (Fig. 7d) was similar for most of the groundwater samples, which could indicate that Ca minerals dissolve similarly in all areas.

The mass ratio of Cl/Br had a relatively wide range and generally increased with salinity, from about 200 to about 10,000 in the more saline groundwater (supplemental Table 1). The higher ratios were detected in groundwater of the pit area and irrigation wells; lower ratios were seen in the dam site samples. Plotting this ratio versus Cl^- (Fig. 7e) showed two different trends. For samples from the dam site and irrigation wells, the trend had a positive slope, while the pit area samples had a slightly negative slope. The first trend indicates that Cl^- does not necessarily correlate with Br^-, while the pit area samples show that Cl^- increased in virtual harmony with Br^-. Based on this observation, there are two different waters: (1) shallow water far from the pit area (dam site and irrigation wells area) and (2) deeper ground water in the pit area (the pit is currently about 120 m deep). Dewatering has caused a reverse hydraulic

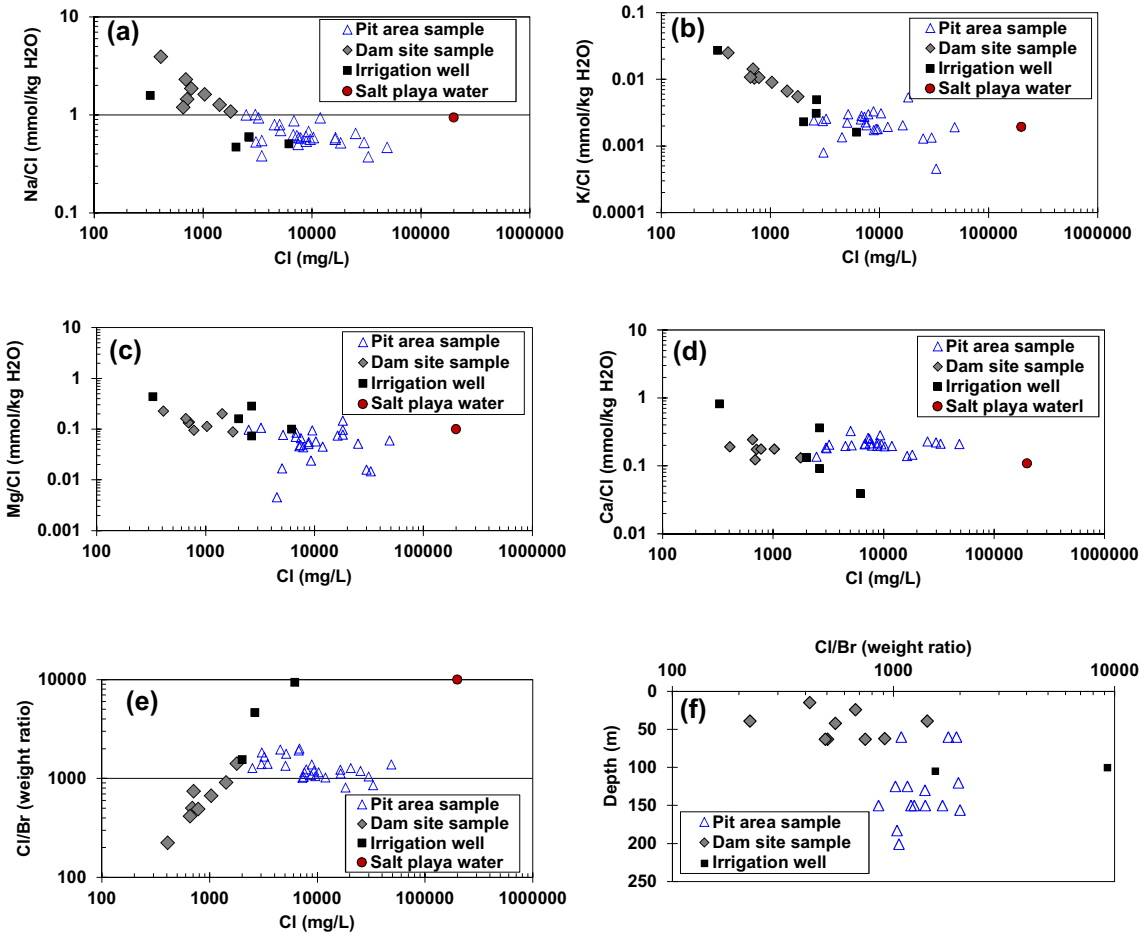

Fig. 7 Plot of molar ions ratio versus Cl^- concentration in mg/L for **a** Na/Cl, **b** K/Cl, **c** Mg/Cl, **d** Ca/Cl, **e** Cl/Br and **f** plot of the groundwater sampling depth versus Cl/Br (weight ratio)

gradient and consequently the intrusion of deep saline water from the Sirjan salt playa into the pit area. The plot of Cl/Br ratios versus sampling depth shows how the ratio increases with depth (Fig. 7f).

The plot of molar concentration of HCO_3^- versus Ca^{2+} and HCO_3^- versus $Ca^{2+} + Mg^{2+}$ are presented in Fig. 8a, b. If these ions were present due to dissolution of calcite or dolomite, the plotted points should follow a 2:1 line. However, this was not the case; instead, there was a negative trend, indicating that other sources of Ca^{2+} and/or Mg^{2+} exist in the area. Dissolution of gypsum or other minerals such as tremolite-actinolite, hornblende, chlorite, epidote, and biotite, and cation exchange can all introduce Ca^{2+} and Mg^{2+} into groundwater.

The relationship between SO_4^{2-} and Ca^{2+} is shown in Fig. 8c. Gypsum dissolution would present a line of 1:1, but this was not the case for most of the samples, and interestingly, the dam site samples plotted to the left of the line, indicating that either that SO_4^{2-} had increased or that Ca^{2+} had decreased. The increase of SO_4^{2-} could be due to dissolution of other SO_4^{2-}-bearing minerals or pyrite oxidation. However, pyrite does not exist in the dam site area and the pH of all samples was near or above 7 (Table 1). The Ca^{2+} decrease could be due to direct cation exchange or dolomitization and/or precipitation of calcite. Since the Na/Cl ratio was greater than 1 for the dam site samples, it appears that Na^+ has been released by silicate weathering; the Ca^{2+} decrease was most probably the result of cation exchange with Na^+. Also, most of the samples from the pit area and the irrigation wells plotted to the right of the 1:1 line (Fig. 8c), further differentiating them from the dam site samples; hence, either SO_4^{2-} concentrations have decreased or Ca^{2+} concentrations have increased, due to dissolution of other Ca^{2+}-bearing minerals beside gypsum, and/or reverse cation exchange.

To clarify whether dissolution of calcite and dolomite produced the additional Ca^{2+} and Mg^{2+}, molar concentrations of $SO_4^{2-} + HCO_3^-$ were plotted versus $Ca^{2+} + Mg^{2+}$

(Fig. 8d). If dissolution of gypsum, calcite, and dolomite were responsible, the samples would have a slope of 7:4, assuming chemical equilibrium.

$$3CO_2 + 3H_2O + CaCO_3 + CaMg(CO_3)_2 + CaSO_4 \leftrightarrow 3Ca^{2+} + Mg^{2+} + 6HCO_3^- + SO_4^{2-}$$

However, most of the samples from the pit area and irrigation wells plot to the right of the 7:4 line. Comparing Fig. 8d, c indicates that the Mg^{2+} increase in the pit area samples was greater than the HCO_3^- increase. This could be due to dissolution of Mg^{2+}-bearing minerals other than dolomite.

Table 1 shows that most samples were supersaturated with respect to calcite and dolomite, indicating the potential precipitation of these minerals in the groundwater. Most samples from the dam site and irrigation wells were under saturated with respect to gypsum and halite, but some samples from closer to the pit are supersaturated with respect to gypsum, and deposition of this mineral is expected.

Stable Isotope Study

Supplemental Table 2 presents the $\delta^{18}O$ and δ^2H values of the area's groundwater and precipitation (Fig. 9a). The local (Sirjan) meteoric water line (LMWL), $\delta^2H = 7.12$ and $\delta^{18}O = 15.92$, were compared with the global meteoric water line (GMWL; Craig 1961). The $\delta^{18}O$ and δ^2H values ranged from −5.6 to −1.5‰ and −35.1 to −21‰, for the groundwater samples; and −15.2 to −1.8‰ and −107.2 to −2.8‰ for the precipitation samples, respectively. All of the groundwater samples plotted below the LMWL. Figure 9b shows three groups of samples:

i. GR1: isotopic compositions close to the LMWL, from the dam site and irrigation wells, far from the pits.
ii. GR2: more enriched samples, including samples from piezometers and pumping wells near the pits.
iii. GR3: samples with the most enriched isotopic composition, including seepage and drainage waters from the hard rock in the bottom of the pits.

Figure 9b and the above proposed grouping could imply a trend in the evolution of the chemical and isotopic composition of the waters, which mixing and/or evaporation play the major roles. Since the water table of the area is more than 60 m below the ground surface, enrichment of groundwater by evaporation is low. However, potential evaporation of runoff prior to recharge into the ground is high due to the area's climate. To clarify the effect of

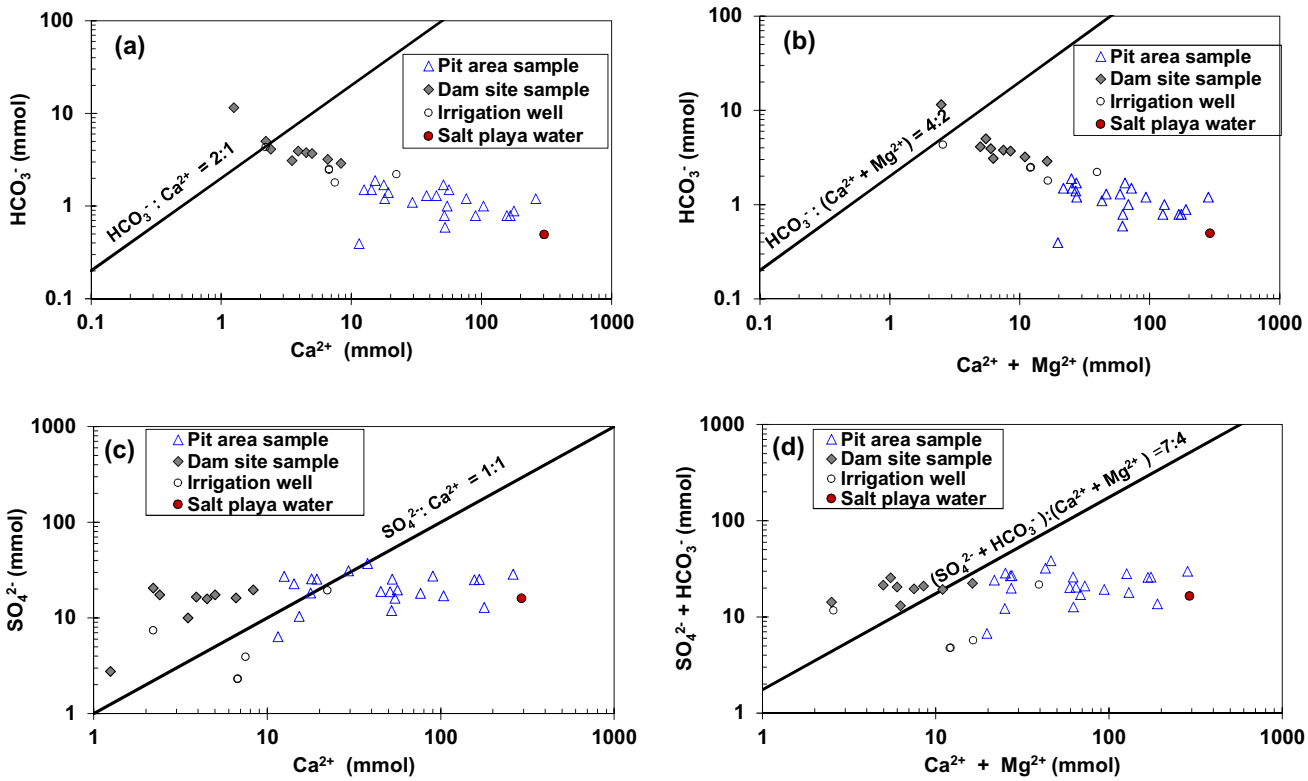

Fig. 8 Plot of molar concentration of: **a** HCO_3^- versus Ca^{2+}, **b** HCO_3^- versus $Ca^{2+} + Mg^{2+}$, **c** SO_4^{2-} versus Ca^{2+}, **d** $SO_4^{2-} + HCO_3^-$ versus $Ca^{2+} + Mg^{2+}$

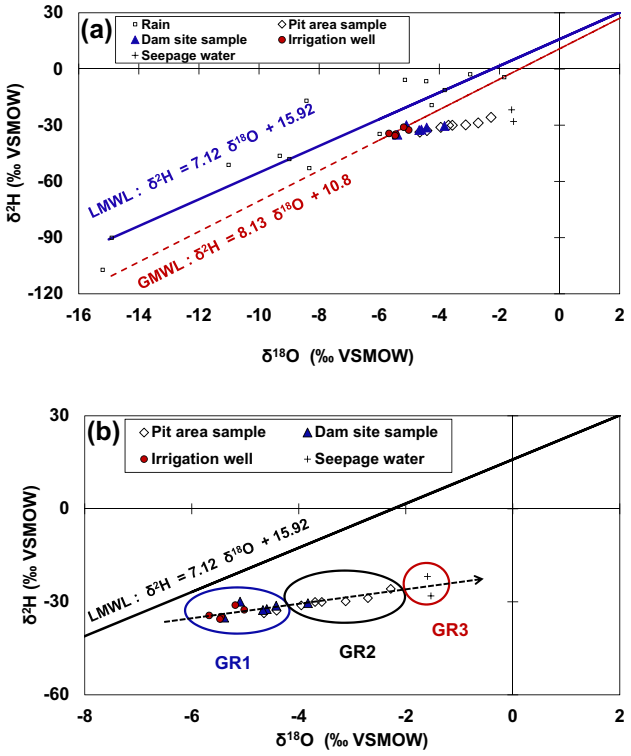

Fig. 9 **a** Stable isotope composition of $\delta^{18}O$ and $\delta^{2}H$ in the groundwater and precipitation samples, LMWL and GMWL. **b** Proposed groups (*GR1*, *GR2* and *GR3*) and trend in water samples of the study area

evaporation on isotopic enrichment of the groundwater, the following approaches were applied:

i) If evaporation from groundwater was a factor, the water would become more saline and $\delta^{2}H$ and Cl^{-} should be highly correlated (Clark and Fritz 1997). Figure 10 shows a weak correlation ($R^2 = 0.093$), indicating that Cl^{-} concentration was not related to $\delta^{2}H$ enrichment. Therefore, the effect of evaporation on enrichment of the stable isotope compositions was low and the increased Cl^{-} concentration could be due to halite dissolution.

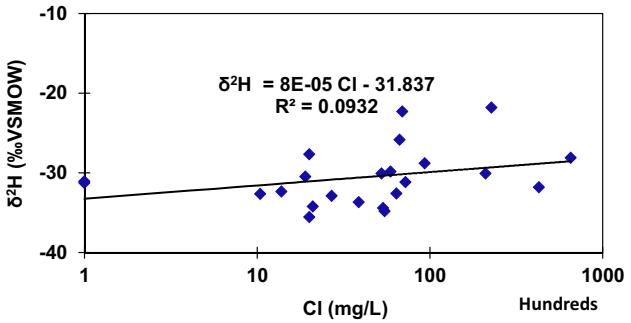

Fig. 10 Relation of $\delta^{2}H$ and Cl^{-} concentrations in the water samples

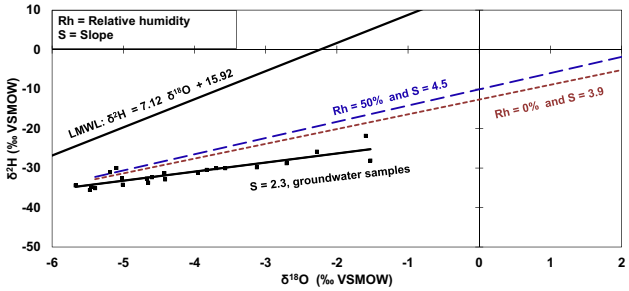

Fig. 11 Slope of trend line in the stable isotope composition of $\delta^{2}H$ and $\delta^{18}O$ in the groundwater samples and slope of isotopic enrichment line by evaporation for a relative humidity of 50 and 0%

ii) If groundwater evaporates in an environment with a relative humidity of 50%, the slope of the enrichment trend line of isotopic composition should be about 4.5; for a relative humidity of 0%, it would be about 3.9 (Clark and Fritz 1997). The $\delta^{2}H$ and $\delta^{18}O$ of the groundwater samples of the study area were plotted beside lines with slopes of 4.5 and 3.9 (Fig. 11). The regression line of the samples has a slope of about 2.3. Since the relative humidity of the study area is about 33%, it was expected that the regression line should plot between these two lines; however, the regression line is below both lines and has a lesser slope. Hence, the enrichment trend has developed by other mechanisms, such as mixing of enriched water with a lower isotopic composition. However, some enrichment could have taken place prior to infiltration, either in the salt playas or during runoff.

Applying the above arguments to the waters of the studied area may clarify that: the waters of group GR1 (Fig. 9b) were similar to the area's precipitation and could be considered as a first end member. Group GR3 samples could represent a second end member, associated with evaporation prior to recharge into groundwater. Group GR2 would result from mixing of these two groups (Fig. 11).

Origin of Groundwater and Conceptual Flow Model

As previously discussed, hydrochemical study of the groundwater implies that four water types exist in the area. From this, one may infer that the groundwater has four different sources. However, dissolution, cation exchange, chemical reactions, and mineral deposition can all change water types. Since the irrigation wells waters near the

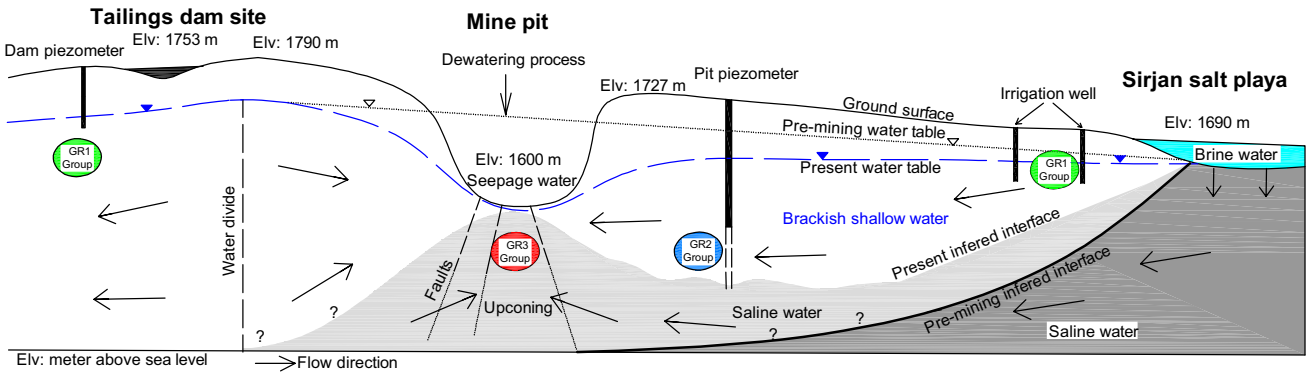

Fig. 12 Proposed conceptual model for circulation of water from the Sirjan salt playa into the mine pit area aquifer

Sirjan salt playa and the sample from the salt playa itself were similar to the groundwater of the pit area, and the groundwater flow direction is from the salt playa area towards the pit (Fig. 6), it was concluded that the water of the pit area are largely supplied by the Sirjan salt playa and the areas in between.

The samples from the dam site were of three water types, all different from those of the pit area (Fig. 3). The flow direction in the dam site is from the northeast towards the southwest (Fig. 6). These clues indicate that groundwater of the dam site has its own origin, and that the lithology of the surrounding geological formations affects their chemical properties and water type. The flow direction in the dam site continues towards the southeast of the area where irrigation well IW4 is located. The similarity of the IW4 water type to that of D6, D7, and D8 supports this indication too. However, the Cl^- content of IW4 increases during the flow path.

Considering the above points of view, a conceptual model for circulation of meteoric water from the Sirjan salt playa into the aquifers of the area through the geological formations, faults, fissures, and porous media of the top alluvium is presented (Fig. 12). This figure shows that the water table gradient and groundwater flow direction in pre-mining operations and dewatering conditions, were from the pit area towards the Sirjan salt marsh, which has the lowest topographic elevation. But due to the mining operations and dewatering process, a cone of depression has gradually developed in the pit area; gradient and flow direction were reversed and intrusion of salt water from the salt playa into the aquifer of the pit area has occurred. Continuation of pumping and drawdown in the upper brackish water of the aquifer also has caused ‘upconing’. As a result, saline water from below the mine is being pumped into the bottom of the pits and mixing of brackish shallow groundwater and saline water from the salt playa, transferred via the faults, fractures, and joints of the deeper hard rock aquifer, is occurred.

The ^{18}O and ^{2}H composition of the groundwater samples confirm the proposed conceptual model and the mixing trend. Considering the relation between ^{18}O and ^{2}H, water group GR1 (Fig. 9) represents shallow groundwater, which is unaffected by mining and possibly resembles groundwater prior to mining and dewatering. Water enriched in isotopes due to evaporation (prior to infiltration from runoff and surface water flows or during residence in the Sirjan salt playa) has entered the lower aquifer, in a way that the intruded saline water enriched in isotopes (represented by the GR3 group) exists below the brackish water. Alternative pumping and the consequence fluctuations of the water table, in addition to diffusion, have caused mixing of the upper fresh-brackish groundwater (GR1) and the more saline groundwater (GR3) of the pit area, producing group GR2.

Conclusions

Additional study of the origins of the groundwater and its various sources was necessary to improve the dewatering of the Golgohar iron ore mine. In addition, the salinity of the water being discharged from the pit and groundwater was high, which affects the environment downstream. Hence, hydrochemistry and chemical processes were used to investigate the effects that dewatering has had on the area’s groundwater.

The hydrochemical studies showed a heterogeneous distribution of salinity in the area’s groundwater. Generally, water with high TDS were found in the mining area’s deep aquifer, while fresh and brackish waters were present in the shallower aquifer in the pit area and samples far from the pit (i.e. the proposed tailings dam site or irrigation wells). Furthermore, the relationships between salinity and depth revealed that a deep saline water reservoir has developed as a result of salt water intrusion from the Sirjan salt marsh, located to the north of the mine. The intruded salt water

has also mixed with fresher, shallower groundwater. Migration of saline water into the pit is a result of the dewatering processes and upconing. However, the groundwater at the proposed tailings dam site has not been affected by the dewatering and salt water intrusion; the groundwater quality there is best explained by long-term mineral dissolution in that vicinity.

Finally, it was determined that the origin of the groundwater in the Golgohar mine pit area is generally the meteoritic water that infiltrates into the shallow groundwater and mixes with more saline water at depth. Most of the discharged groundwater from the mine comes from the Sirjan salt marsh, flowing through the faults, fractures, and joints in the deep hard rock aquifer. So, to prepare a sound plan for additional dewatering, it will be essential to pay attention to fault zones in the hard rock aquifer.

Acknowledgements This work was partially supported by the Golgohar Mining and Industrial Company. The isotopes were analyzed under the supervision of Prof. Michael Schneider at the Institute für Geologische, Freie Universitat, Berlin. We thank the editors and the anonymous reviewers for their constructive comments.

References

Alcalá FJ, Custodio E (2008) Using the Cl/Br ratio as a tracer to identify the origin of salinity in aquifers in Spain and Portugal. J Hydrol 359:189–207

Allen DM, Lepitre ME (2004) Use of Pb, ^{18}O, and ^{2}H isotopes in mining-related environmental studies. Mine Water Environ 23:119–132

Amajor LC, Gbadebo AM (1992) Oil field brines of meteoric and connate origin in the eastern Niger delta. J Pet Geol 15(4), p 481–488

APHA (1989) Standard methods for the examination of water and wastewater. 17th edn. American Public Health Association, New York City, p 4–197

Appelo CAJ, Postma D (2005) Geochemistry, groundwater and pollution, 2nd edn. Balkema, Rotterdam

Brahim YA, Benkaddour A, Agoussine M, Lemkademe AA, Yacoubi LA, Bouchaou L (2015) Origin and salinity of groundwater from interpretation of analysis data in the mining area of Oumjrane, Southeastern Morocco. Environ. Earth Sci 74(6):4787–4802

Carpenter AB (1978) Origin and chemical evolution of brines in sedimentary basins. Okl Geol Surv Circ 79, 60–77

Cartwright I, Weaver TR, Fifield LK (2006) Cl/Br ratios an environmental isotopes as indicators of recharge variability and groundwater flow: an example from the southeast Murray Basin, Australia. Chem Geol 231:38–56

Clark ID, Fritz P (1997) Environmental isotopes in hydrogeology. Lewis Publication, New York City

Craig H (1961) Isotopic variations in meteoric waters. Science 133:1702–1703

Currell Matthew J, Dahlhaus P, Hiroyuki L (2014) Stable isotopes as indicators of water and salinity sources in a southeast Australian coastal wetland: identifying relict marine water, and implications for future change. Hydrogeol J 23:235–248

Dixon W, Chiwell B (1992) The use of hydrochemical sections to identify recharge areas and saline intrusions in alluvial aquifers, southeast Queensland, Australia. J Hydrol 135:259–274

Faye S, Maloszewski P, Stichler W, Gaye CB (2005) Groundwater salinization in the Saloum (Senegal) delta aquifer: minor elements and isotopic indicators. Sci Total Environ 343:243–259

Freeman JT (2007) The use of bromide and chloride mass ratios to differentiate salt-dissolution and formation brines in shallow ground waters of the western Canadian sedimentary basin. Hydrogeol J 15:1377–1385

Gammons CH (2006) Geochemistry of perched water in an abandoned underground mine, Butte, Montana. Mine Water Environ 25:114–123

Gammons CH, Metesh JJ, Snyder DM (2006) A survey of the geochemistry of flooded mine shaft water in Butte, Montana. Mine Water Environ 25:100–107

Ghiglieri G, Carletti A, Pittalis D (2012) Analysis of salinization processes in the coastal carbonate aquifer of Porto Torres (NW Sardinia, Italy). J Hydrol 432–433:43–51

Giménez E, Morell I (1997) Hydrogeochemical analysis of salinization processes in the coastal aquifer of Oropesa (Castellon, Spain). Environ Geol 29:118–131

Han D, Kohfahl C, Song X, Xiao G, Yang J (2011) Geochemical and isotopic evidence for paleo-seawater intrusion into the south coast aquifer of Laizhou Bay, China. Appl Geochem 26:863–883

Iribar V, Ábalos B (2011) The geochemical and isotopic record of evaporite recycling in spas and salterns of the Basque Cantabrian basin, Spain. Appl Geochem 26:1315–1329

Jahanshahi R, Zare M (2016) Hydrochemical investigations for delineating salt-water intrusion into the coastal aquifer of Maharlou Lake, Iran. J Afr Earth Sci 121:16–29

Kharaka YK, Maest AS, Carothers WW, Law LM, Lamothe PJ, Fries TL (1987) Geochemistry of metal-rich brines from central Mississippi Salt Dome Basin, USA. Appl Geochem 2:543–561

Leybourne MI, Goodfellow WD (2007) Br/Cl ratios and O, H, C, and B isotopic constraints on the origin of saline waters from eastern Canada. Geochim Cosmochim Acta 71:2209–2223

Magaritz M, Luzier JE (1985) Water–rock interactions and seawater–freshwater mixing effects in the coastal dune aquifer, Coos Bay, Oregon. Geochim Cosmochim Acta 49:2515–2525

Mohammadi Z, Zare M, Sharifzade B (2012) Delineation of groundwater salinization in a coastal aquifer, Bousheher, South of Iran. Environ Earth Sci 67(5):1473–1484

Möller P, Rosenthal E, Geyer S, Flexer A (2007) Chemical evolution of saline waters in the Jordan-Dead Sea transform and in adjoining areas. Int J Earth Sci 96(3):593–597

Mondal NC, Singh VS, Saxena VK, Singh VP (2011) Assessment of seawater impact using major hydrochemical ions: a case study from Sadras, Tamilnadu, India. Environ Monit Assess 177:315–335

Morell I, Giménez E, Esteller MV (1996) Application of principal components analysis to the study of salinization on the Castellon Plain (Spain). Sci Total Environ 177:161–171

Mücke A, Younessi R (1994) Magnetite-apatite deposits (Kiruna-type) along the Sanandaj-Sirjan zone and in the Bafq area, Iran, associated with ultramafic and calcalkaline rocks and carbonatites. Miner Petrol 50: 219–244

Nadler A, Magaritz M, Mazor E (1981) Chemical reactions of seawater with rocks and freshwater experimental and field observations on brackish waters in Israel. Geochim Cosmochim Acta 44:879–886

Park SC, Yun ST, Chae GT et al (2005) Regional hydrochemical study on salinization of coastal aquifers, western coastal area of South Korea. J Hydrol 313:182–194

Parkhurst DL, Appelo CAJ (1999) User's guide to PHREEQC (version 2): a computer program for speciation, batch reaction, one-dimensional transport and inverse geochemical calculations. USGS WRI report 95-4259, Denver

Richter BC, Kreitler CW (1993) Geochemical techniques for identifying sources of ground-water salinization. CRC Press, Boca Raton

Singh AK, Mahato MK, Neogi B, Mondal GC, Singh TB (2011) Hydrogeochemistry, elemental flux, and quality assessment of mine water in the Pootkee-Balihari mining area, Jharia Coalfield, India. Mine Water Environ 30:197–207

Sprenger C, Parimala Renganayaki S, Schneider M, Elango L (2014) Hydrochemistry and stable isotopes during salinity ingress and refreshment in surface- and groundwater from the Arani–Koratallai (A–K) basin north of Chennai (India). Environ Earth Sci 73:7769–7780

Sukhija BS, Varma VN, Nagabhushanam P, Reddy DV (1996) Differentiation of paleomarine and modern seawater intruded salinities in coastal groundwaters (of Karaikal and Tanjavur, India) based on inorganic chemistry, organic biomarker fingerprints and radiocarbon dating. J Hydrol 174:173–201

Tijani MN (2004) Evolution of saline waters and brines in the Benue-Trough, Nigeria. Appl Geochem 19:1355–1365

Yidana SM, Yidana A (2010) An assessment of the origin and variation of groundwater salinity in southeastern Ghana. Environ Earth Sci 61:1259–1273

Zhang G, Deng W, Yang YS, Salama RB (2007) Evolution study of a regional groundwater system using hydrochemistry and stable isotopes in Songnen Plain, northeast China. Hydrol Process 21:1055–1065